COVER SURFACES AS A NEW TECHNIQUE FOR 3D GPR IMAGE ENHANCEMENT. ARCHAEOLOGICAL APPLICATIONS

J.A. Peña [a,b,*] and T. Teixidó [a]
[a] Instituto Andaluz de Geofísica, Universidad de Granada, Spain
[b] Departamento de Prehistoria y Arqueología, Universidad de Granada, Spain
Corresponding author. E-mail address: peruano@ugr.es

ABSTRACT

Currently, there are several ways to present 3D Ground Penetrating Radar (GPR) results: time or depth slices, a mixture of radargram-slice images, GPR reflectivity maps and GPR isosurface images. In this study, we review these image-based rendering techniques and present a new alternative technique to construct 3D images that improve the visualisation of GPR results. We call this new representation technique "3D GPR cover surfaces".

To evaluate the quality of these 3D cover surfaces compared to other standard imaging techniques, we use a GPR dataset from the Iberian site of La Escuera (Alicante, Spain). These data were acquired with a 400-MHz antenna on profiles with 0.5 m spacing. We show images of the resulting 3D cover surfaces and demonstrate that they are similar to a stratigraphic archeological excavation.

Keywords: 3D GPR data processing, 3D GPR images, 3D GPR cover surfaces, stratigraphic archeological excavation.

1. INTRODUCTION

Present standards of 3D GPR imaging are based on pseudo 3D methodologies that use data acquired in parallel profiles form, although in some instances, the data may have irregular spacing. In archaeological sites, structures at depths minor than 3 m may require detailed horizontal exploration. Antennas with frequencies of 250 to 500 MHz are commonly used with line spacing of 0.25 m to 1 m, with 0.5 m being the most common spacing. Because GPR signals are emitted and received at every 2 to 5 cm, the data are oversampled along each profile [1].

After GPS surveying, we model a data volume in terms of space (x_i, y_i, z_i) and reflection amplitude (A_i), with the goal of generating several images that provide guidance for archaeological excavation. In Figure 1, we show the pseudo 3D GPR scheme, where the

radargram profiles, A'(x, z), are processed similarly to zero-offset seismic sections (staked sections), and the resulting volume A(x, y, z) is calculated by interpolation algorithms for obtaining 3D GPR images [2].

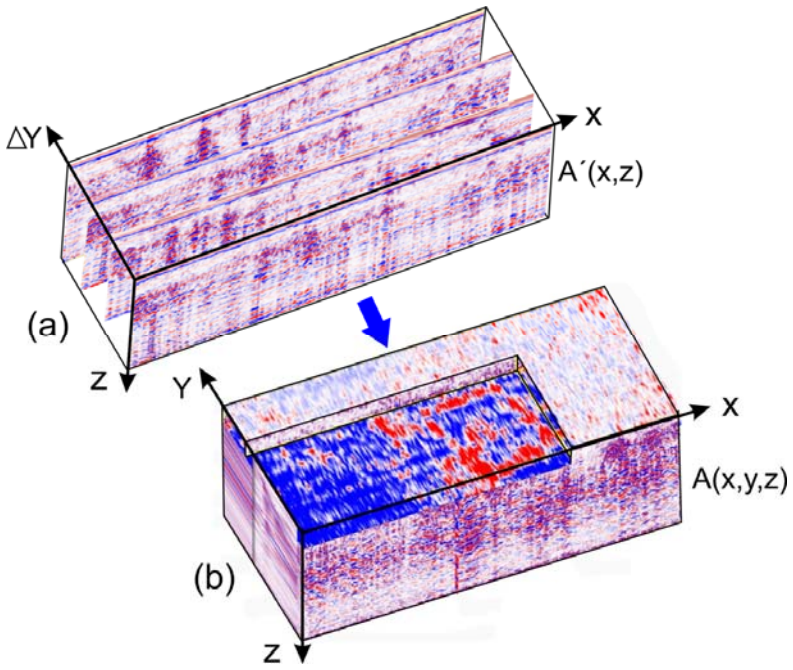

Figure 1. Pseudo-3D GPR scheme. (a) The survey zone is sampled by closely spaced parallel profiles (Δy). The radargram profiles are placed according to the geometry of their acquisition. A' (x, z) is the reflection amplitude field for each GPR profile. (b) After processing the raw dataset, reflections between neighbouring profiles are interpolated, generating a volume A (x, y, z) whose results are ready to be analysed through different GPR imaging techniques.

Alternatively, analysis can be carried out with 3D GPR ultra-dense grids, called "true 3D GPR", by recording nearby profiles in perpendicular directions [3, 4]. However, this technique requires a large data acquisition effort and presents some methodological issues for obtaining unaliased 3D images at depths suitable for archeological uses [5, 6]. This is mainly due to two aspects of the data acquisition: the Nyquist condition for heterogeneous medium (particularly for dipping reflectors) and the Fresnel criterion above 3 m depth.

2. SELECTED EXAMPLE: LA ESCUERA - IBERIAN ARCHEOLOGICAL SITE

The survey area is located on the outskirts of the city of San Fulgencio (Alicante, Spain). This Iberian site is from IV-II BC, coinciding with the Second Punic War. Excavation near the geophysical study area shows a temple with an orthogonal plan in most of its dependences [7] and an urban area where some domestic buildings are against a fortified wall [8]. The average depth of buried structures is between 0.65 to 1.5 m, and most are made of masonry and ashlar (Figure 2a).

The field work was carried out in June 2008. A 400-MHz antenna (Figure 2b) was used due to its optimum tradeoff between penetration and resolution to best define the archaeological features of interest at this site. Because pseudo 3D GPR is a widely used method in the identification of buried archaeological structures [9, 10, 11, 12], the 495 m^2 (33 m x 15 m) of the study area was explored by parallel profiles spaced 0.5 m in Y-direction. The following acquisition parameters were selected: 512 samples/trace, 4 stacks/trace, 60 ns duration and a trace trigger interval of 2 cm.

(a) (b)

Figure 2. (a) Iberian structure excavated near the study area. (b) Basic GSSI equipment for data acquisition: a 400-MHz antenna with an odometer and recording unit attached to the back. A guideline at every 50 cm (profile separation) was used to place each profile.

Raw radargrams show good signal penetration and numerous reflectors. The processing flow [13] for raw datasets consists of a time correction, background removal, predictive deconvolution, Kirchoff migration, band-pass filtering and linear gain correction (Figure 3). In this case, topographic and tilt-antenna corrections are not needed. Finally, two different types of data volumes are generated for comparing the pseudo 3D images. The first is generated directly after the flow processing, and the second is created by spatially averaging the squared wave amplitudes (Hilbert transform). In the two volumes, the main geometry of the reflectors coincides and is coherent with previous archaeological information. However, the Hilbert transform volume data set provides better images, and we use it in this study. For the two-way time to depth conversion, we use a dielectric constant of 10; this adimensional value is obtained through lithologic considerations and averaging of collapsed major hyperbolas.

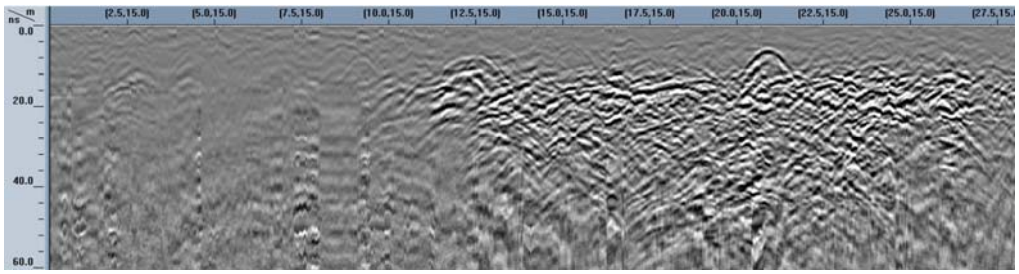

Figure 3. Processed radargram prior to migration and Hilbert transform. The archaeological structures are mainly located on the right-hand side of the studied survey and are imaged mainly between 15 to 40 ns.

3. STANDARD 3D IMAGING TECHNIQUES

In archaeological 3D GPR surveying, the resulting volume is usually presented in the form of radargrams in cross-section, time slices and interpretative maps; although overlain reflectivity maps, isosurface renderings and shaded relief maps are also included on some occasions [14]. Integrated views of different elements in the same graphic (e.g. 3D volume slices, topography, isosurfaces and chair cutaways) are preferred.

3.1. Time (or depth) slices (Figure 4) are maps on which the reflection amplitudes have been projected at a specified time (or depth), with a selected time interval (or thickness) [15]. This results in a collection of maps for different times (T_i) or depths (Z_i) (i = 0, 1,...,n) in terms of amplitude $A_H(x,y)$. These are the horizontal projections of all amplitudes collected for a specified thickness Δt_i (or Δz_i) around T_i (or Z_i), i.e. $T_i \pm \Delta t_i$ or ($Z_i \pm \Delta z_i$) for i = 0 1,...,n, where n is the number of slices. These GPR slice maps are the most used because they show easily the depth evolution of buried structures, including their size, shape and location. Time or depth GPR slices represent an improvement in imaging because subtle features that are indistinguishable on radargrams can be see and interpreted through these slice maps. Animations of time slices are usually generated as the final step for basic 3D GPR data visualisation. Image and video files can be created generated directly or with specialised or commercial software. When the GPR results are good enough, the slices can be shown as relief slice maps (or warped slice maps), which display slices in three dimensions (Figure 5).

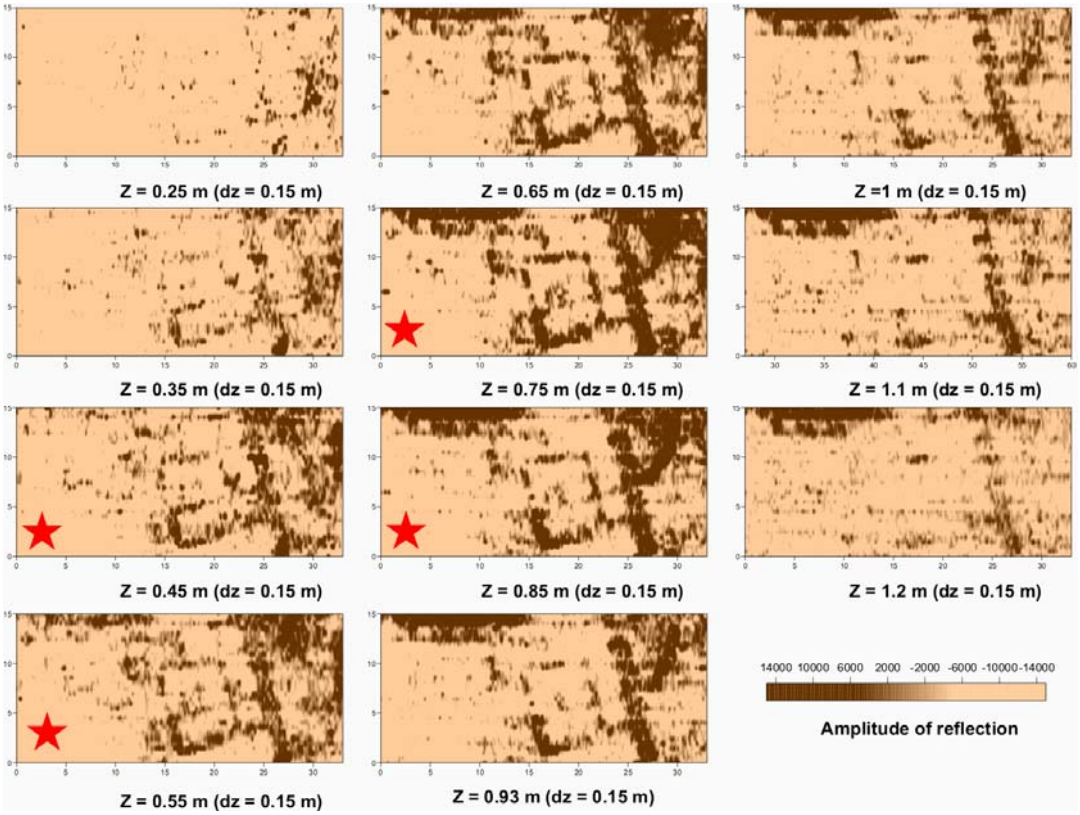

Figure 4. Consecutive depth slices of the survey. Z_i ranges from 0.25 to 1.2 m depth in 10 cm intervals (Δz) for the 8 first slices and 0.15 m intervals for deeper slices. Slices with red stars are selected for overlay analysis.

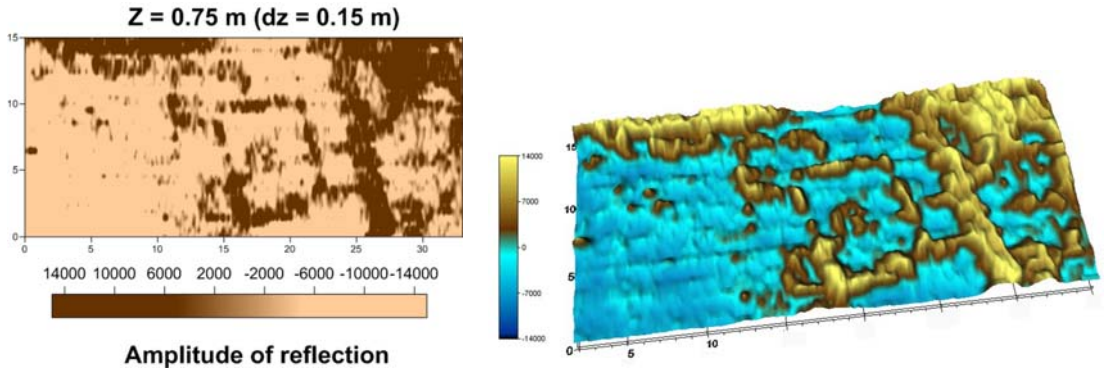

Figure 5. (a) GPR slice at 75 cm depth in horizontal projection mode. (b) The same GPR slice shown in warped mode. Both images describe the same $A_H(x,y)$ wave field at specific depth Z_i; (0.75 m) respective colour scales indicate the amplitude of reflection.

3.2. Overlay analysis is a graphic method developed by Goodman et al. [16] that synthesises reflections at various travel times onto a single composite time or depth slice map. At survey sites, the buried structures of interest may not be located at the same depth, and the time slices can hide some features due to their thickness, leading to erroneous interpretations. In overlay analysis, the strongest and weakest reflectors at the depth of each slice are assigned specific colours. Because the grid spacing is the same for all slices, we can select the reflection amplitude components that are to be included in the cumulative final image (slices marked with red stars in Figure 4). The strongest reflector A'(x,y) at each depth is displayed (Figure 6a). After inspecting these individual maps showing the overlay components from each level separately, the progressive overlay images A*(x,y) are generated (Figure 6b). This technique allows the linkage of structures buried at different depths, and it can be a very useful processing tool in archaeological interpretation.

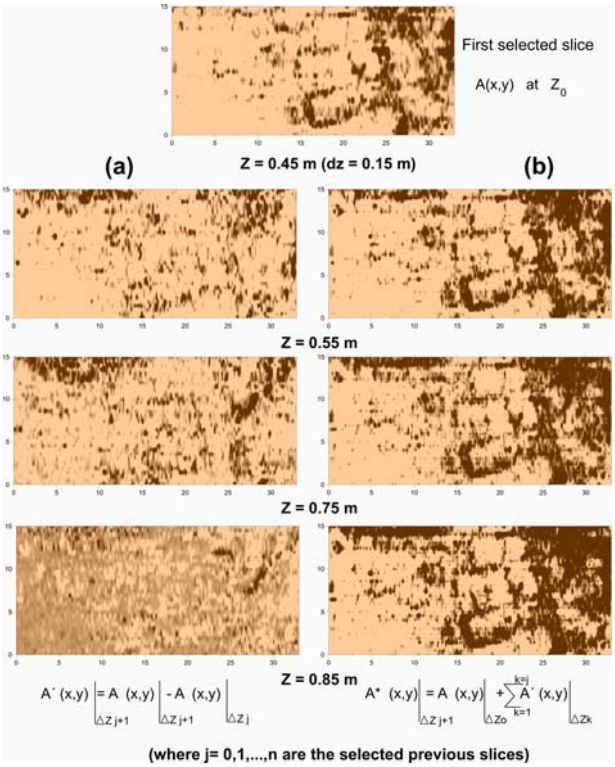

Figure 6.

(a) Overlay slice analysis showing the individual components of the strongest reflectors at each depth. For the shallowest slice, the complete image is displayed, A(x,y); in the next slice, only the illuminated areas that have stronger reflections than the previous map are included, A'(x,y). In the third image, all areas on the map have larger reflections than on the previous two maps. This process is continued down to the desired depth. (b) Progressive overlay images containing reflections, A*(x,y), from 45 to 85 cm depth.

3.3. 3D amplitude isosurface imaging is also a powerful technique for archeological interpretation of 3D GPR data [17]. 3D amplitude isosurface rendering displays amplitudes of equal value in the GPR study volume. Shading is usually used to illuminate these surfaces, giving the appearance of real archeological structures. The threshold amplitude setting is crucial for obtaining useful results. Values of 60 to 70% of the maximum amplitude value usually provide the best results; however, any particular case must be studied separately.

Illumination is often added to the isosurface calculation to emphasise the features contained in the data volume (Figure 7). This three-dimensional display of GPR data simulates the transmission and absorption of light through points in the volume. Light rays are cast through the volume, where amplitudes within the volume may reflect or absorb light. The colour of an individual pixel on the screen is computed by combining contributions from each particle intersecting the ray. This allows the viewing of heterogeneity within objects with appropriate adjustment of the opacity. Commercial packages software, such as GPR-Slices v6.0 or Voxler v2 [18], are used for these representations. Numerous disciplines other than geophysics are also interested in this 3D data imaging technique, such as computational fluid dynamics, medical imaging, meteorology and chemistry.

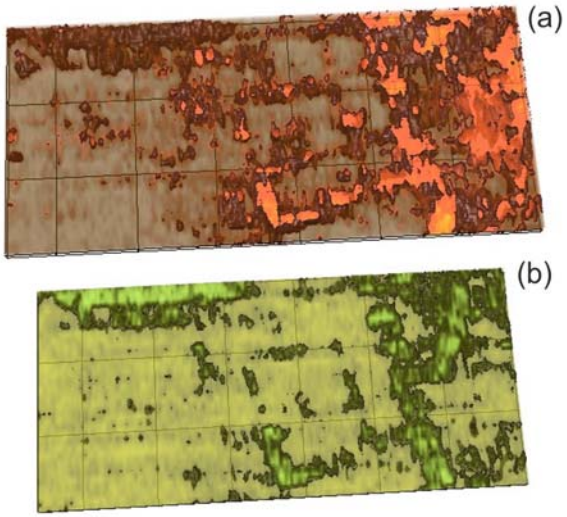

Figure 7. Integrated views of 3D amplitude isosurfaces and volume renderings for two depths. (a) 3D amplitude isosurface results between 0.25 m and 0.8 cm depth, for A > 60% $A_{max.}$ (b) 3D amplitude isosurface results between 0.8 m and 1.2 m depth, for A > 65% A_{max}.

4. 3D-GPR COVER SURFACES

The called "3D GPR cover surface" is a new representation technique to construct 3D images at improves the visualisation of GPR results. We describe its calculation scheme below:

Similar to overlay analysis, first we generated depth slices with a narrow thickness (Δz). The thickness and the number of slices depend on the selected depth within the GPR volume and the spatial distribution of the reflector bodies (Figure 8a and 8b). Typically, the thickness is around 10% of the selected depth and we generated 15 to 20 slices per meter.

In second steep we compared each amplitude point $A_0(x_i, y_i)$ belonging to the initial slice (Z_0) with selected threshold amplitude A*. If the amplitude reflection $A_0(x_i, y_i) \geq$ A*, the point (x_i,y_i,z_0) is retained and the inspection of homologous vertical points (x_i,y_i,z_j), j≠0 stops. If $A_0(x_i, y_i) <$ A*, the search extends from the second selected slice, $A_1(x_i, y_i)$ at Z_1 depth, and we compare $A_1(x_i, y_i)$ with A* on the same criteria. This recursive process continues to the selected depth of interest (i = 0, 1, ...,n), where n is the deepest slice. This inspection is performed for all (x_i,y_i) points in each slice.

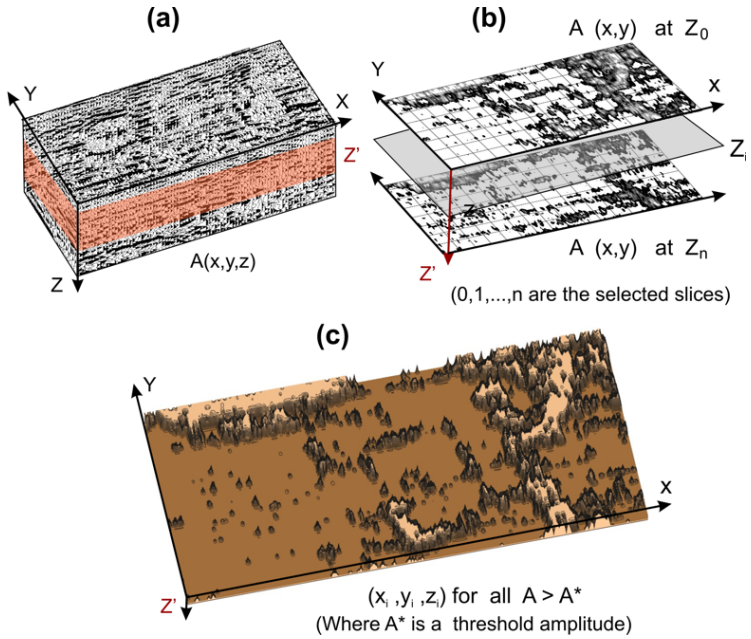

Figure 8. Process for calculating a specific 3D cover surface. (a) First, select a subset of 3D data. (b) Second, generate consecutive depth slices, starting at Z_0 depth and continuing to Z_n, the final depth. (c) Third, we retain the point (x_i,y_i,z_i) nearest to the surface that have amplitude larger than a threshold value A*.

The final result is a set of points (x_i,y_i,z_i) representing the first maximum amplitude detected from the "ground" in each point of the 3D GPR subset (Figure 8c). We name this set of points the "GPR cover surface" because the obtained image is similar to a sheet that is overlain on points that exceed a threshold amplitude value. Note that, while the slices and the overlay analysis are 2D images of amplitude A(x,y), the cover surface is a 3D relief (x_i,y_i,z_i) and this topographic surface has some similarity to a stratigraphc archeological excavation; this is also known as excavation by natural levels. In this type of excavation, when an archeologist detects a positive structure, related to a maximum reflection amplitude, he can continue digging around it without crossing the location of the reflection, contouring the structure's shape for this particular body.

Because we start with a set of depth slices where the amplitudes (which may have been normalised) are spread over a wide range of values, a methodological question arises as to what threshold amplitude value is appropriate in order to 3D cover surfaces can be representative of buried archaeological structures. Through many archeological surveys, we have established that the best threshold amplitude (A*) is generally between the 60% to 85% of the maximum total

amplitude (A_{max}). We also find that A* is strongly dependent on the specific reflectivity of the study area. Thus, in archeological sites where the buried structures have a large dielectric contrast to the filling materials, A* can be large (near 80% to 90% of A_{max}) because the reflections tend to be strong. In places with low dielectric impedance, A* should be lower (near 60% to 70% of A_{max}). In practice, we have established A* as an input parameter and, for a given set of depth slices, we generated 3D cover surfaces with different threshold values and selected the best image (Figure 9). Another result of setting the A* value is that, in most occasions, it mitigates the background noise due to scattered reflections (e.g. dispersed stones and collapsed materials) or the artefact produced for lost signal/noise relation ship at large depths.

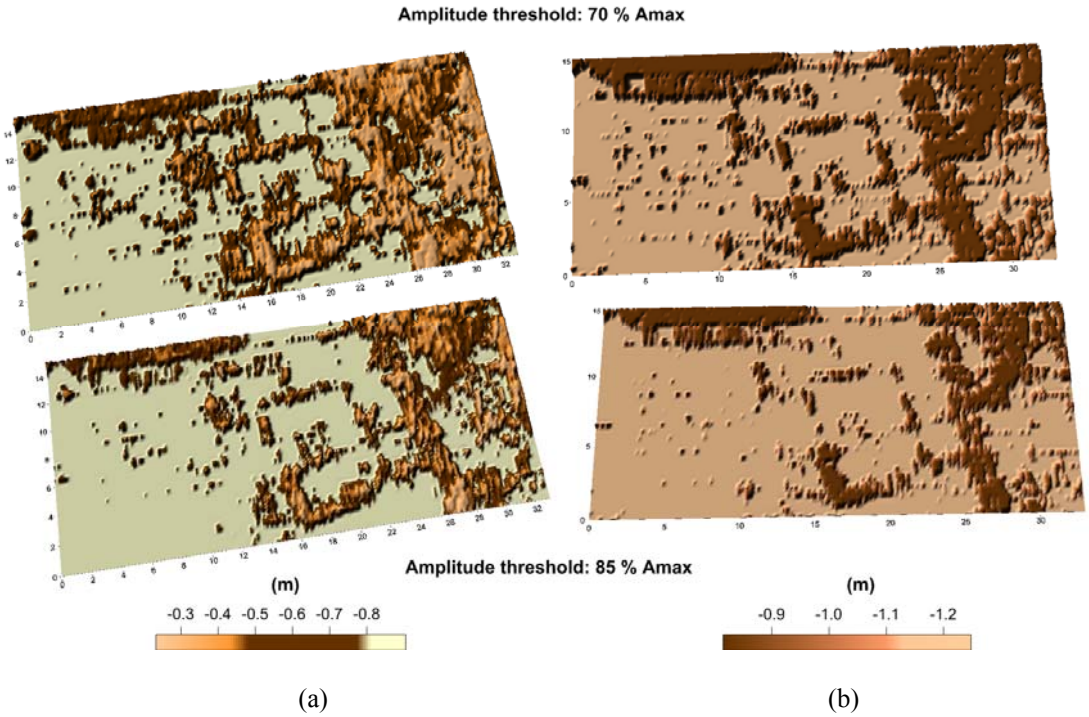

(a) (b)

Figure 9. 3D cover surfaces for two depths. (a) Cover surface between 0.25 m and 0.8 m depth and (b) cover surfaces between 0.8 m and 1.2 m depth. Surfaces for the two levels are generated with two threshold amplitudes of 70% and 85%, respectively.

Although both 3D isosurface amplitude images and 3D cover surface images are similar (see Figure 7a versus Figure 9a), the 3D isosurface amplitude displays all amplitudes at a given "volume depth", showing all envelopes of same cutoff amplitude value. These represent closures of these envelopes that often do not properly represent archeological structures. For example, the GPR response to a wall is given by a reflection at the top of the wall and one at the bottom, while the spaced between the top and bottom of them is not reflective. Therefore, in 3D amplitude isosurface display, it will generate two separated envelopes for the same wall (top and bottom reflections); in contrast, the 3D cover surface reproduces the correct outline of the wall (the envelope of the first reflection until the bottom). However, in areas with collapses or flat structures over others structures below them, the cover surfaces cannot image these deeper structures. Here the geophysicist can establish the depth ranges for each cover surface to image the relevant archeological information. In this sense, the cover surfaces shown in Figure 9a

show the first level of archeological structures (mainly walls and collapsed materials), and cover surfaces in Figure 9b show the bases of the largest walls and large semicircular structure beneath the collapsed materials, located at the right of the survey.

5. CONCLUSIONS

Geophysical surveying of archeological sites requires that images contain as much information as possible and are easily understood and interpreted by archaeologists. This is particularly important in 3D GPR surveys because the high experimental sampling (ns or cm) can provide very high resolution results. This is the concern of much of the current 3D GPR research: how can we obtain better GPR images from a given dataset? In this study, we present a new method that can be used in such direction.

The code to calculate 3D cover surfaces is programmed in Visual Basic (v6.0), and the results are displayed in the Surfer (v9.11) [19] commercial package. The "singularity" of this work is not due to the difficulty in generating 3D cover surfaces; its "singularity" is own idea resulting of our collaboration with archeologists, in the effort to provide clearly 3D GPR images.

6. ACKNOWLEDGEMENTS

The GPR equipment used in this study was provided through an ERDF project (European Regional Development Fund) during 2002-2004. The GPR data used in this study were obtained at the Escuera archeological site. This site is led by Dr. Lorenzo Abad and Dr. Feliciana Sala of the Prehistory, Archeology, and Ancient History Department of the Alicante University (Spain).

7. REFERENCES

[1, 15] L.B. Conyers. Ground-penetrating radar for archeology. Altamira press, PO Box 317 Oxford OX2 9RU, UK, 2004.

[2] X. Feng, J. Fujiwara, Z. Zhou, T. Kobasayashi and M. Sato. Imaging algorithm of hald-held GPR MD sensor system (ALIS). Proceedings 5794, pp 1192-1199. SPIE Photonics West, San Francisco, California USA, 2005.

[3] M. Grasmueck, R. Weger and H. Horstmeyer. Full-resolution 3D GPR imaging, Geophysics,70 (1), pp12-1.9. 2005

[4] M. Grasmueck, D.A. Viggiano. Integration of Ground-Penetrating Radar and Laser Positioning Sensors for Real-Time 3-D Data Fusion, IEEE Transactions on Geoscience and Remote Sensing, 45, 45 (1), pp.130-137.2007

[5] A. Novo, H. Lorenzo, F.I. Rial, M. Pereira and M. Solla. Ultra-dense grid strategies for 3D GPR in Archaeology. Proceedings of 12th International Conference on Ground Penetrating Radar, Birmingham, UK. CD-ROM. 2008.

[6] A. Novo, M. Grasmueck, D.A. Viggiano, H. Lorenzo. 3D GPR in Archaeology: What can be gained from dense Data Acquisition and Processing?, Proceedings of 12th International Conference on Ground Penetrating Radar, Birmingham, UK. CD-ROM. 2008.

[7] S. Nordström. Excavaciones en el poblado de La Escuera (San Fulgencio, Alicante), T.V. del S.I.P., 34, Valencia.1967.

[8] L. Abad, I. Grau, F. Sala and J. Moratalla. Ancient Trade in South-eastern Iberia: the Lower Segura River as Focus of Exchange Activities. *Ancient West & East*, volume 2, no. 2, Leiden-Boston pp 265-287. 2003.

[9] J. Leckebusch. Ground-Penetrating Radar: A Modern Three-dimensional Prospection Method, Archaeological Prospection, 10, pp. 213-240. 2003.

[10] A.D. Booth, N. Linford, R. Clark and T. Murray. Three-dimensional,Multi-offset Ground-penetrating Radar Imaging of Archaeological Targets, Archaeological Prospection, 15, pp. 93-112. 2008.

[11] J.A. Peña, T. Teixidó, E. Carmona and M. Sierra, M. Prospección magnética y radar 3D como métodos para obtener información *a priori* en la planificación de una excavación arqueológica. Caso de estudio: Yacimiento del Cortijo de Quintos (Córdoba, España), 6ª Asamblea Hispano-Portuguesa de Geodesia y Geofísica, 11-14 Febrero, Tomar, Portugal, pp. 231-232. 2008

[12] T. Teixidó and J.A. Peña. Prospección GPR en varios sectores del yacimiento arqueológico de Utica (Túnez). AGA-78 Internal document of History, Geography and Art History Department. Almería University (Spain). 2010.

[13] D.J. Daniels (Editor). Ground-penetrating radar -2nd ed.-, The Institution of Electrical Engineers, London, UK. 2004.

[14] A.L. Novo. 3D GPR Imaging for Archeological Prospection, Department of Natural Resources and Environmental Engineering. University of Vigo Spain, Doctoral Thesis, 153 pp. 2009.

[16] D. Goodman, J. Steinberg , B. Damiata, Y. Nishimura, K. Schneider, H. Hiromichi, N. Higashi. GPR Overlay Analysis for Archaeological Prospection, Proceedings of the 11th International Conference on Ground Penetrating Radar, Columbus, Ohio, USA. CD-ROM. 2006.

[17] D. Goodman. GPR_slice V6.0 Manual. From http://WWW.gpr-survey.com, January 2009

[18] Voxler v2. Volumetric Visualization Package. Golden Software, Inc. http://www.goldensoftware.com/ . 2006-2010.

[19] Surfer v9.11. Surface Mapping System. Golden Software Inc. http://www.goldensoftware.com. August 2010.